Photoelasticity and acousto-optic diffraction in piezoelectric semiconductors

Susumu Fukuda, Toshihiko Karasaki, Tadashi Shiosaki, and Akira Kawabata
Department of Electronics, Faculty of Engineering, Kyoto University, Kyoto 606, Japan
(Received 18 June 1979)

Contributions from the free-carrier screened indirect photoelastic effect and from the free-carrier density fluctuations to the photoelasticity in piezoelectric semiconductors have been considered by taking account of the existence of both electrons and holes. Explicit expressions for the effective photoelastic constants corresponding to these contributions have been derived on the basis of the small-signal acousto-electric theory. The results obtained are applicable either to extrinsic or to intrinsic semiconductors. The numerical evaluation of these contributions has been carried out by taking tellurium as an example. In accordance with the theoretical prediction, an appreciable diffraction ascribable to the free-carrier density fluctuations has been observed in the acousto-optic diffraction experiments.

I. INTRODUCTION

An elastic deformation accompanying an acoustic mode traveling in a medium gives rise to optical scattering phenomena known as Brillouin scattering or acousto-optic diffraction. The physical mechanism of these scattering phenomena in an anisotropic crystal can best be described in terms of the time-space fluctuations in the inverse dielectric constant of the crystal. Especially, as discussed by Keller,[1-3] in strongly piezoelectric semiconductors three effects can contribute significantly to these fluctuations:

$$\Delta(1/\kappa)_{ij}^{t} = \Delta(1/\kappa)_{ij}^{d} + \Delta(1/\kappa)_{ij}^{in} + \Delta(1/\kappa)_{ij}^{fc}, \tag{1.1}$$

where $\Delta(1/\kappa)_{ij}$ is the change in the inverse dielectric constant at an optical frequency caused by the elastic deformation. (Hereafter a dielectric constant at an optical frequency will be designated by κ_{ij} and we shall retain ϵ_{ij} to mean that at an acoustic frequency.) The first term $\Delta(1/\kappa)_{ij}^{d}$ represents the direct photoelastic effect arising from the fluctuations in the strain (or equivalently, the Pöckels photoelasticity) and from the mean rotation of the volume element. The formulation of the direct effect was derived by Nelson and Lax[4,5] on a phenomenological basis as

$$\Delta(1/\kappa)_{ij}^{d} = p_{(ij)(kl)} S_{(kl)} + p_{(ij)[kl]} R_{[kl]} = p_{(ij)kl} u_{k,l}, \tag{1.2}$$

where the summation convention has been used. In the first term $p_{(ij)(kl)}$ is the Pöckels photoelastic tensor component and $p_{(ij)[kl]}$ in the second term represents the photoelastic tensor due to the rotational contribution. The infinitesimal strain and mean rotation are defined, respectively, by

$$S_{(kl)} \equiv \tfrac{1}{2}(u_{k,l} + u_{l,k}) \tag{1.3}$$

and

$$R_{[kl]} \equiv \tfrac{1}{2}(u_{k,l} - u_{l,k}). \tag{1.4}$$

Parentheses enclosing subscripts indicate symmetry upon interchange of the subscripts, while bracketed subscripts indicate antisymmetry upon interchange. The gradient of the displacement vector u_k of the acoustic wave is denoted by $u_{k,l} \equiv \partial u_k / \partial x_l$. The antisymmetric part $p_{(ij)[kl]}$ can be calculated simply from the optical dielectric tensor[4,5]:

$$p_{(ij)[kl]} = \tfrac{1}{2}[(1/\kappa)_{il}\delta_{kj} + (1/\kappa)_{lj}\delta_{ik} - (1/\kappa)_{ik}\delta_{lj} - (1/\kappa)_{kj}\delta_{il}]. \tag{1.5}$$

The second term on the right-hand side of Eq. (1.1), $\Delta(1/\kappa)_{ij}^{in}$, represents the indirect photoelastic effect, i.e., the succession of the piezoelectric and electro-optic effects. This effect includes the screening caused by the free carriers and can be calculated from the acousto-electrically induced self-consistent electric field due to the piezoelectric coupling. The third term, $\Delta(1/\kappa)_{ij}^{fc}$, gives the change of the inverse dielectric constant caused by the fluctuation in the free-carrier densities, i.e., an acoustic wave may be accompanied by free-carrier density waves arising also from the piezoelectric coupling. Accordingly, the second and third terms are significant only when the acoustic wave is piezoelectrically active or, equivalently, when the acoustic wave induces a longitudinal self-consistent electric field. Contributions from the deformation-potential coupling may be ignored, since in strong piezoelectric semiconductors contributions from the piezoelectric coupling dominate these by many orders of magnitude. Appearance of the third term was first theoretically predicted by Proklov, Shkerdin, and Gulyaev[6] and experimentally verified by Proklov, Mirgorodsky, Shkerdin, and Gulyaev[7] in an n-type CdS crystal.

Because both the second and third terms on the

right-hand side of Eq. (1.1) are tensor functions of the elastic deformation (the appropriate independent elastic variable in this case is the strain), it is possible to define effective photoelastic constants for these two terms. An explicit expression for the photoelastic constant for the indirect effect was derived by Nelson and Lax[5] for the case without free-carrier screening and by Sasaki, Tsubouchi, Chubachi, and Mikoshiba[8] for the case with screening. The latter authors started from the Hutson-White formulation[9,10] for the acousto-electric interaction assuming the existence of only one kind of free carrier, and therefore it applies only to extrinsic semiconductors. On the other hand, Keller[2] gave rather general expressions for the dielectric fluctuations of the second and third terms in Eq. (1.1), but assumed also only one kind of free carrier.

In contrast to the previous works above this paper takes account of the existence of both electrons and holes and derives the expressions for effective photoelasticity that are applicable to piezoelectric semiconductors in either an intrinsic or an extrinsic conduction regime. The theoretical treatment presented in Sec. II A is based upon the linear acousto-electric theory originally developed by Fink and Quentin[11] taking two kinds of free carriers into account. The treatment is therefore valid for the cases in which the small-signal theory applies. The derived results predict that in intrinsic semiconductors considerable cancellation may occur between photoelasticity due to electron-density fluctuation and that due to hole-density fluctuation. In Sec. II B we apply the results to tellurium, one of the strongest piezoelectric semiconductors. Finally, in Sec. III acousto-optic diffraction experiments of 10.6-μm infrared light from a CO_2 laser are carried out using a tellurium crystal in an intrinsic conduction regime at room temperature. In accordance with the theoretical prediction, an appreciable diffraction ascribable to the free-carrier density fluctuations is observed.

II. THEORETICAL

A. Photoelasticity in piezoelectric semiconductors

In this section we derive the expression for the effective photoelastic constants corresponding to the second and third terms on the right-hand side of Eq. (1.1). In the following treatment the recombination between electrons and holes will be neglected. This assumption is legitimate in tellurium, where $\tau_{rec} \sim 10^{-6}$ sec,[11] which is much longer than the period of the acoustic wave we shall be concerned with. In order to derive the effective photoelastic tensors with full symmetry, the tensor notations will be retained throughout.

The basic equations that describe the acousto-electric interaction are the mechanical wave equations, the Maxwell equations, and the piezoelectric equations of state[11]:

$$T_{pq} = c_{pqkl} S_{kl} - e_{spq} E_s , \tag{2.1}$$

$$D_i = e_{imn} S_{mn} + \epsilon_0 \epsilon_{ki} E_k , \tag{2.2}$$

where T_{pq} is the stress, S_{kl} is the strain, c_{pqkl} is the elastic stiffness constant, e_{imn} is the piezoelectric constant, and ϵ_{ki} is the dielectric constant at an acoustic frequency. The subscripts refer to the usual rectangular crystallographic coordinates. An acoustic wave propagating in the medium creates an instantaneous local modulation of the free-carrier densities: neglecting trapping effect,

$$n' = n_0 + n , \tag{2.3}$$

$$p' = p_0 + p , \tag{2.4}$$

where n_0 and p_0 are the equilibrium density of electrons and holes in the absence of an acoustic wave and n and p represent their instantaneous local changes. Poisson's equation is satisfied separately for the two kinds of free carriers:

$$\frac{\partial D_i^n}{\partial x_i} = -qn, \quad \frac{\partial D_i^p}{\partial x_i} = qp , \tag{2.5}$$

and

$$D_i = D_i^n + D_i^p , \tag{2.6}$$

where the superscripts n and p denote the component due to electrons and to holes, respectively. The equations of charge continuity are

$$\frac{\partial J_j^n}{\partial x_j} = q \frac{\partial n}{\partial t} , \quad \frac{\partial J_j^p}{\partial x_j} = -q \frac{\partial p}{\partial t} . \tag{2.7}$$

The total current density is

$$J_j = J_j^n + J_j^p , \tag{2.8}$$

with

$$J_j^n = \sigma_{kj}^n E_k + q \mathfrak{D}_{ij}^n \frac{\partial n}{\partial x_i} \tag{2.9}$$

and

$$J_j^p = \sigma_{kj}^p E_k - q \mathfrak{D}_{ij}^p \frac{\partial p}{\partial x_i} , \tag{2.10}$$

where $\mathfrak{D}_{ij}^n$ and $\mathfrak{D}_{ij}^p$ are the diffusion constants, the equilibrium conductivities are

$$\sigma_{kj}^n = q n_0 \mu_{kj}^n, \quad \sigma_{kj}^p = q p_0 \mu_{kj}^p , \tag{2.11}$$

and the nonlinear terms containing nE_k and pE_k have been dropped compared with the other terms. Equations (2.1)–(2.10) can be solved by introducing plane-wave time and space dependences such as

$$E_k = E_k^0 \exp[j(k_i^a x_i - \omega t)] \tag{2.12}$$

and

$$n = n^0 \exp[j(k_i^a x_i - \omega t)], \tag{2.13}$$

where k_i^a and ω are the wave vector and the frequency of the acoustic wave. The piezoelectrically induced self-consistent longitudinal electric field is then obtained as

$$E_r = -\frac{a_r a_l e_{lmn} S_{mn}}{\epsilon_0 a_k \epsilon_{kp} a_p} \left(1 + \frac{j(\omega_C^n/\omega)}{1 + j(\omega/\omega_D^n)} + \frac{j(\omega_C^p/\omega)}{1 + j(\omega/\omega_D^p)}\right)^{-1}, \tag{2.14}$$

where the dielectric relaxation frequencies are

$$\omega_C^n = \frac{a_l \sigma_{ij}^n a_j}{\epsilon_0 a_k \epsilon_{kl} a_l}, \quad \omega_C^p = \frac{a_l \sigma_{ij}^p a_j}{\epsilon_0 a_k \epsilon_{kl} a_l}, \tag{2.15}$$

and the diffusion frequencies are

$$\omega_D^n = v^2/a_i \mathfrak{D}_{ij}^n a_j = qv^2/a_i \mu_{ij}^n a_j k_B T, \tag{2.16}$$

$$\omega_D^p = v^2/a_i \mathfrak{D}_{ij}^p a_j = qv^2/a_i \mu_{ij}^p a_j k_B T. \tag{2.17}$$

Here v is the acoustic velocity, a_i is the component of the directional cosine of the acoustic wave vector, and k_B is the Boltzmann constant. The local fluctuations in the free-carrier densities due to bunching are then

$$n = \frac{a_l e_{lmn} S_{mn}}{qv} \frac{\omega_C^n}{[1 + j(\omega/\omega_D^n)]} \times \left(1 + \frac{j(\omega_C^n/\omega)}{1 + j(\omega/\omega_D^n)} + \frac{j(\omega_C^p/\omega)}{1 + j(\omega/\omega_D^p)}\right)^{-1} \tag{2.18}$$

and

$$p = -\frac{a_l e_{lmn} S_{mn}}{qv} \frac{\omega_C^p}{[1 + j(\omega/\omega_D^p)]} \times \left(1 + \frac{j(\omega_C^n/\omega)}{1 + j(\omega/\omega_D^n)} + \frac{j(\omega_C^p/\omega)}{1 + j(\omega/\omega_D^p)}\right)^{-1}. \tag{2.19}$$

From Eq. (2.14) the change of the inverse dielectric constant arising from the indirect effect, i.e., the second term on the right-hand side of Eq. (1.1), can be written

$$\Delta(1/\kappa)_{ij}^{\text{in}} = \gamma_{ijr} E_r = -\frac{\gamma_{ijr} a_r a_l e_{lmn} S_{mn} A}{\epsilon_0 a_k \epsilon_{kp} a_p} \equiv p_{ijmn}^{\text{in}} S_{mn}, \tag{2.20}$$

with

$$A = \left(1 + \frac{j(\omega_C^n/\omega)}{1 + j(\omega/\omega_D^n)} + \frac{j(\omega_C^p/\omega)}{1 + j(\omega/\omega_D^p)}\right)^{-1}, \tag{2.21}$$

where γ_{ijr} is the electro-optic constant measured at constant strain. The effective photoelastic constant defined in Eq. (2.20) is then given by

$$p_{ijmn}^{\text{in}} = \frac{\gamma_{ijr} a_r a_l e_{lmn} A}{\epsilon_0 a_k \epsilon_{kp} a_p}. \tag{2.22}$$

The third term on the right-hand side of Eq. (1.1) can be obtained through the relation for infrared radiation[12]:

$$\kappa_{ij} = \kappa_{ij}^0 - \frac{q^2 n'}{\epsilon_0 \omega_o^2} \left(\frac{1}{m_n}\right)_{ij} - \frac{q^2 p'}{\epsilon_0 \omega_o^2} \left(\frac{1}{m_p}\right)_{ij}, \tag{2.23}$$

where n' and p' have been defined in Eqs. (2.3) and (2.4), κ_{ij}^0 is the dielectric constant in the absence of free carriers, ω_o is the optical frequency, and m_n and m_p are the electron and the hole effective mass, respectively. Differentiating Eq. (2.23) with respect to n' and p', we obtain

$$\Delta\kappa_{ij}^{\text{fc}} \equiv \Delta\kappa_{ij}^n + \Delta\kappa_{ij}^p = -\kappa_{ij}^n (n/n_0) - \kappa_{ij}^n (p/p_0), \tag{2.24}$$

where

$$\kappa_{ij}^n = \frac{q^2 n_0}{\epsilon_0 \omega_o^2} \left(\frac{1}{m_n}\right)_{ij}, \quad \kappa_{ij}^p = \frac{q^2 p_0}{\epsilon_0 \omega_o^2} \left(\frac{1}{m_p}\right)_{ij}, \tag{2.25}$$

and n and p have been derived in Eqs. (2.18) and (2.19). To obtain the change in the inverse dielectric constant, we shall employ the following identity equation:

$$\Delta(1/\kappa)_{ij} = -(1/\kappa)_{im} \Delta\kappa_{mn} (1/\kappa)_{nj}. \tag{2.26}$$

In the crystal symmetries except for triclinic and monoclinic systems the coordinate system we have referred to above agrees with the dielectric principal axes, so that Eq. (2.26) is reduced to the simple form

$$\Delta(1/\kappa)_{ij} = -\frac{\Delta\kappa_{ij}}{\kappa_{ii}\kappa_{jj}}. \tag{2.27}$$

Substitution of Eq. (2.24) into Eq. (2.27) yields

$$\Delta(1/\kappa)_{ij}^{\text{fc}} = \frac{\kappa_{ij}^n}{\kappa_{ii}\kappa_{jj}} \left(\frac{n}{n_0}\right) \delta_{ij} + \frac{\kappa_{ij}^p}{\kappa_{ii}\kappa_{jj}} \left(\frac{p}{p_0}\right) \delta_{ij} \equiv p_{ijmn}^{\text{fc}} S_{mn}. \tag{2.28}$$

The effective photoelastic constant is then written

$$p_{ijmn}^{\text{fc}} \equiv p_{ijmn}^n + p_{ijmn}^p = \frac{a_l e_{lmn} A}{\kappa_{ii}\kappa_{jj} qv} \left(\frac{\kappa_{ij}^n}{n_0} \frac{\omega_C^n}{1 + j(\omega/\omega_D^n)} - \frac{\kappa_{ij}^p}{p_0} \frac{\omega_C^p}{1 + j(\omega/\omega_D^p)}\right) \delta_{ij}. \tag{2.29}$$

Because the right-hand side of Eq. (2.29) contains κ^n_{ij} and κ^p_{ij}, which are inversely proportional to the square of the optical frequency, ω_o^2, the photoelasticity arising from the free-carrier density fluctuations in some favorable cases may become comparable to or even larger than the two other contributions for the measurements using a sufficiently long optical wavelength (10.6-μm light of a CO_2 laser, for example).

For piezoelectric semiconductors in the extrinsic conduction regime (p-type, for example), after putting the equilibrium electron density n_0 equal to zero as compared with p_0, Eqs. (2.22) and (2.29) become

$$p^{\text{in}}_{ijmn} = -\frac{\gamma_{ijr} a_r a_l e_{lmn}}{\epsilon_0 a_k \epsilon_{kp} a_p} \frac{1+j(\omega/\omega^p_D)}{1+j(\omega^p_C/\omega+\omega/\omega^p_D)} \tag{2.30}$$

and

$$p^{\text{fc}}_{ijmn} = -\frac{a_l e_{lmn} \kappa^p_{ij} \delta_{ij}}{\kappa_{ii}\kappa_{jj} q v p_0} \frac{\omega^p_C}{1+j(\omega^p_C/\omega+\omega/\omega^p_D)} . \tag{2.31}$$

Equation (2.30) is reduced to the expression derived by Sasaki *et al.*[8] Equations (2.29) and (2.31) indicate that the conductivity dependence of p^{fc}_{ijmn} between intrinsic and extrinsic semiconductors is considerably different. In particular, for the intrinsic case in which the relation $n_0 = p_0$ holds between the two equilibrium carrier densities, p^n_{ijmn} and p^p_{ijmn} defined in Eq. (2.29) have the absolute values which are, in general, not very much different from each other, while the phase angle between them is always greater than $\frac{1}{2}\pi$ and less than π. Especially when $\omega^n_D \sim \omega^p_D$, the phase angle cannot deviate very much from π, regardless of ω. The maximum deviation of the phase angle from π occurs at the acoustic frequency of $\omega = (\omega^n_D \omega^p_D)^{1/2}$. As a result, considerable cancellation is expected between the photoelasticity due to the electron-density fluctuation and that due to the hole-density fluctuation. This behavior, as suggested by Eqs. (2.18) and (2.19), indicates that the electron bunching and the hole bunching always occur nearly π out of phase, provided that $\omega^n_D \sim \omega^p_D$. If $\omega^n_D = \omega^p_D$, the phase angle between p^n_{ijmn} and p^p_{ijmn} is exactly π, so that the most effective cancellation takes place.

It is understood from Eqs. (1.2), (1.5), (2.22), and (2.29) that the photoelastic tensors corresponding to the different physical origins possess different symmetries and show different dependences on the acoustic and optical frequencies. This permits a powerful experimental technique to measure each contribution separately. For acoustic frequencies $\omega \ll \omega^{n,p}_C$, $\omega^{n,p}_D$, Eqs. (2.22) and (2.29) can be approximated as

$$p^{\text{in}}_{ijmn} = j\frac{\gamma_{ijr} a_r a_l e_{lmn}}{\epsilon_0 a_k \epsilon_{kp} a_p} \frac{\omega}{\omega^n_C + \omega^p_C} \tag{2.32}$$

and

$$p^{\text{fc}}_{ijmn} = -j\frac{a_l e_{lmn}}{\kappa_{ii}\kappa_{jj} q v} \frac{\omega}{\omega^n_C + \omega^p_C} \left(\frac{\kappa^n_{ij}\omega^n_C}{n_0} - \frac{\kappa^p_{ij}\omega^p_C}{p_0} \right) \delta_{ij} , \tag{2.33}$$

indicating that the absolute values of both photoelastic constants increase in proportion to ω. For sufficiently high frequencies $\omega \gg \omega^{n,p}_C$, $\omega^{n,p}_D$ the free-carrier screening rapidly diminishes and p^{in}_{ijmn} approaches its high-frequency limit,

$$p^{\text{in}}_{ijmn} = -\frac{\gamma_{ijr} a_r a_l e_{lmn}}{\epsilon_0 a_k \epsilon_{kp} a_p} , \tag{2.34}$$

which is in agreement with the expression obtained by Nelson and Lax[5] in the limit of zero conductivity. On the other hand, $|p^{\text{fc}}_{ijmn}|$ decreases in inverse proportion to ω as

$$p^{\text{fc}}_{ijmn} = -j\frac{a_l e_{lmn}}{\kappa_{ii}\kappa_{jj} q v} \frac{1}{\omega} \left(\frac{\kappa^n_{ij}\omega^n_C\omega^n_D}{n_0} - \frac{\kappa^p_{ij}\omega^p_C\omega^p_D}{p_0} \right) \delta_{ij} . \tag{2.35}$$

These frequency dependences will be considered in more detail in Sec. II B by taking tellurium as an example.

B. Photoelasticity and acousto-optic Bragg diffraction in tellurium

Tellurium is a semiconducting material with a trigonal crystal structure belonging to class-32 symmetry and shows p-type extrinsic conduction below its Hall-reversal temperature of about 200°K. Since tellurium is one of the most highly piezoelectric materials, it shows remarkable nonlinear conduction due to the acousto-electric effect at low temperature.[13-17] Ultrasonic amplification in this material was achieved for the first time by Ishiguro and Tanaka[13] and by Ishiguro *et al.*[18] using a shear ultrasonic wave of 45 MHz propagating along the y axis at 77°K. These previous experimental results suggest that appreciable dielectric modulation due to the piezoelectric coupling should be observed when piezoelectrically active ultrasonic waves traverse the material. Recently the acousto-optic properties of tellurium were studied in detail by the present authors at the 10.6 μm wavelength of CO_2 laser light.[19,20]

The symmetric part $p_{(ij)(kl)}$ of the photoelastic tensor for the direct effect in crystals with class 32 symmetry is given by[21]

$$\begin{bmatrix} p_{11}^s & p_{12} & p_{13} & p_{14} & 0 & 0 \\ p_{12} & p_{11} & p_{13} & -p_{14} & 0 & 0 \\ p_{31} & p_{31} & p_{33} & 0 & 0 & 0 \\ p_{41} & -p_{41} & 0 & p_{44} & 0 & 0 \\ 0 & 0 & 0 & 0 & p_{44} & p_{41} \\ 0 & 0 & 0 & 0 & p_{14} & \frac{1}{2}(p_{11}-p_{12}) \end{bmatrix}, \quad (2.36)$$

(8 independent components)

where the contracted matrix notation is used and the superscript s is attached to clarify its symmetric property. Equation (1.5) gives the antisymmetric part $p_{(ij)[kl]}$ as

$$p_{(13)[13]} = p_{(23)[23]} = \tfrac{1}{2}(1/N_e^2 - 1/N_o^2), \quad (2.37)$$

where N_o and N_e are the ordinary and the extraordinary refractive indices, respectively. The other antisymmetric components are identically zero in this crystal class. For tellurium, $N_o = 4.7939$ and $N_e = 6.2433$ at 10.6 μm.[22] Then the value of Eq. (2.37) reduces to -0.0089.

The photoelastic tensor p_{ijmn}^{in} for the indirect effect is determined from Eq. (2.22) using the dielectric-constant and piezoelectric-constant tensors of class 32 as

$$\begin{bmatrix} p_{11}^{in} & -p_{11} & 0 & p_{14} & p_{15} & p_{16} \\ -p_{11} & p_{11} & 0 & -p_{14} & -p_{15} & -p_{16} \\ 0 & 0 & 0 & 0 & 0 & 0 \\ p_{41} & -p_{41} & 0 & p_{44} & p_{45} & p_{46} \\ p_{46} & -p_{46} & 0 & p_{45} & p_{55} & p_{56} \\ p_{16} & -p_{16} & 0 & p_{15} & p_{65} & p_{66} \end{bmatrix}. \quad (2.38)$$

(12 independent components)

In a similar way Eq. (2.29) determines p_{ijmn}^{fc} as

$$\begin{bmatrix} p_{11}^{fc} & -p_{11} & 0 & p_{14} & p_{15} & p_{16} \\ p_{11} & -p_{11} & 0 & p_{14} & p_{15} & p_{16} \\ p_{31} & -p_{31} & 0 & p_{34} & p_{35} & p_{36} \\ 0 & 0 & 0 & 0 & 0 & 0 \\ 0 & 0 & 0 & 0 & 0 & 0 \\ 0 & 0 & 0 & 0 & 0 & 0 \end{bmatrix}. \quad (2.39)$$

(8 independent components)

As pointed out by Nelson and Lax,[5] because of the presence of the acoustic wave-vector direction a_l in p_{ijmn}^{in} as shown by Eq. (2.22), it does not transform as a simple fourth-rank tensor. It is instead a tensor function of the acoustic wave-vector direction. The same situation holds also in p_{ijmn}^{fc}, which has been derived thus far in this paper.

Since p_{ijmn}^{fc} is equal to zero if $i \neq j$, it is understood that the acousto-optic diffraction of an incident light caused by the free-carrier density fluctuations does not accompany a right-angle rotation of the polarization plane. In the Bragg-diffraction limit,[23] therefore, when the polarization vector of the incident light lies in the plane perpendicular to the optic axis in an optically uniaxial crystal like tellurium, the diffraction will take the form of isotropic Bragg diffraction.[24] On the other hand, anisotropic Bragg diffraction takes place when the polarization plane rotates at a right angle to that of the incident light (i.e., $i \neq j$), and refractive indices for both lights differ from each other.[25]

Starting from Eq. (3.41) in Ref. 5, an expression for the diffracted optical intensity from the Bragg diffraction can be derived under the phase-matching condition for plane waves. Ignoring the incident optical wave depletion due to the diffraction, we obtain

$$I_D = I_I \frac{\pi^2}{2\lambda_0^2} \left(\frac{N_I^3(\theta_I) N_D^3(\theta_D) p_{\text{eff}}^2}{\rho v^3} \right) \frac{P_A}{LH} \frac{L^2}{\cos^2\theta_D}, \quad (2.40)$$

where the subscripts I and D indicate the quantities relating to the incident and the diffracted light, respectively, N is the refractive index, P_A is the acoustic power, L and H are respectively the width and the height of the cross section of the acoustic column where the direction of L lies in the scattering plane and is normal to the acoustic wave vector, ρ is the density, v is the acoustic velocity, λ_0 is the wavelength of the diffracted light in vacuum, θ is the angle between the optical wave vector and the normal to the acoustic wave vector, and p_{eff} is the effective photoelastic constant[26] given by

$$p_{\text{eff}} = \left| d_m^D p_{mnkl} d_n^I a_l b_k \right|, \quad (2.41)$$

where d_m^D and d_n^I are unit vectors in the direction of the electric displacement of the diffracted and incident waves. a_l and b_k are unit vectors in the direction of the acoustic wave vector and material displacement. p_{mnkl} is a relevant photoelastic tensor component given by Eqs. (2.22), (2.29), and (2.36)–(2.39). In the derivation of Eq. (2.40) we have made the approximation that $\cos\delta_D \simeq 1$ and $\cos\delta_I \simeq 1$, where $\delta_{D,I}$ are the angles between the optical Poynting vector and the wave vector. Equation (2.40) is essentially the same as those usually referred to in experimental determinations of acousto-optic material figures of merit [Eq. (3) in Ref. 27, for example] except that the latter

expressions often contain some ambiguous notations for refractive indices and photoelastic constant.

In order to utilize Eqs. (2.40) and (2.41), it is necessary to determine the frequency dependence of the angle of incidence θ_I and the corresponding angle of diffraction θ_D under the phase-matching condition (or, equivalently, the Bragg condition), which can be derived simply from a consideration of energy and pseudomomentum conservation as the following well-known equations[24]:

$$\sin\theta_I = \frac{\lambda_0}{2N_I(\theta_I)v}\left(f + \frac{v^2}{f\lambda_0^2}\left[N_I^2(\theta_I) - N_D^2(\theta_D)\right]\right) \tag{2.42}$$

and

$$\sin\theta_D = \frac{\lambda_0}{2N_D(\theta_D)v}\left(f - \frac{v^2}{f\lambda_0^2}\left[N_I^2(\theta_I) - N_D^2(\theta_D)\right]\right), \tag{2.43}$$

where $f(=\omega/2\pi)$ is the acoustic frequency.

In the acousto-optic diffraction experiments we shall describe below, a shear ultrasonic wave propagating along the crystallographic y axis with the velocity of 1390 m/sec at room temperature was used as one of the highly piezoelectrically active acoustic waves in tellurium. This wave has its displacement vector parallel to the x axis, so that the mean rotation of the volume element defined by Eq. (1.4) is reduced to $R_{[12]}$. Because Eq. (2.37) reveals that there are no nonzero antisymmetric photoelastic components corresponding to $R_{[12]}$, we can neglect the rotational contribution; consequently, the only relevant variable we must retain to describe the elastic deformation is the strain S_{12}. The experimental geometry is shown in Fig. 1, in which the angles measured outside the medium are determined by Snell's law as

$$\theta_I' = \sin^{-1}[N_I(\theta_I)\sin\theta_I] \tag{2.44}$$

and

$$\theta_D' = \sin^{-1}[N_D(\theta_D)\sin\theta_D]. \tag{2.45}$$

The incident optical beam was transmitted in the y-z plane and ordinarily polarized parallel to the x axis. Therefore, in an isotropic Bragg case the polarization of the diffracted light is also parallel to the x axis and both $N_I(\theta_I)$ and $N_D(\theta_D)$ coincide with the ordinary index given by N_o, being independent of θ_I and θ_D. Equations (2.42) and (2.43) are then reduced to

$$\sin\theta_I = \sin\theta_D = \lambda_0 f/2N_o v. \tag{2.46}$$

For anisotropic Bragg diffraction, on the other hand, the polarization vector of the diffracted light lies in the y-z plane and Eqs. (2.42) and (2.43) are simply modified by putting $N_I(\theta_I) = N_o$ and

$$N_D(\theta_D) = 1/[(\cos\theta_D/N_o)^2 + (\sin\theta_D/N_e)^2]^{1/2}.$$

Figure 2 shows the thus calculated external angles θ_I' and θ_D' for both isotropic and anisotropic Bragg

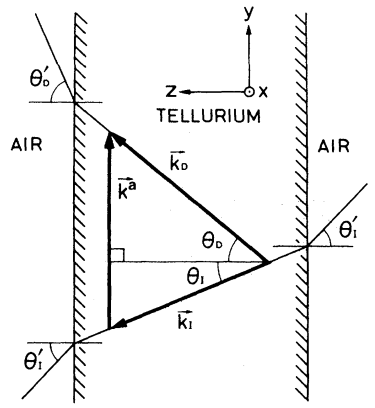

FIG. 1. Schematic illustration of the wave-vector diagram employed in the acousto-optic diffraction experiments. $\vec{k}_I$ and $\vec{k}_D$ are the wave vectors of the incident and diffracted light, respectively. θ_I and θ_D are the angles of incidence and diffraction measured inside the crystal, while θ_I' and θ_D' are those measured outside. $\vec{k}^a$ is the wave vector of the shear acoustic wave propagating along the y axis. The coordinate axes denote the crystallographic orientation for the tellurium sample. The diffraction plane is parallel to the y-z plane.

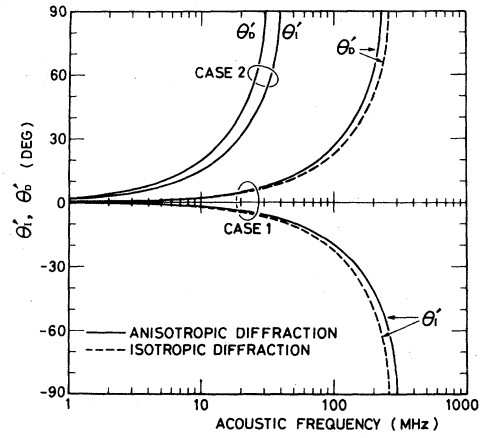

FIG. 2. Calculated angles of incidence and diffraction outside the tellurium crystal at 10.6 μm as a function of frequency of a shear acoustic wave propagating in the y direction with displacement parallel to the x axis. The incident light is an ordinary wave polarized along the x axis and the diffraction plane lies in the y-z plane. Solid curves are obtained for anisotropic Bragg diffraction, while broken curves are isotropic Bragg diffraction. Two kinds of solutions are denoted respectively by "case 1" and "case 2" for the anisotropic diffraction.

TABLE I. Pöckels photoelastic constants in tellurium.

$\lvert p_{11}^s \rvert$	$\lvert p_{12}^s \rvert$	$\lvert p_{13}^s \rvert$	$\lvert p_{31}^s \rvert$	$\lvert p_{33}^s \rvert$	$\lvert p_{14}^s \rvert$	$\lvert p_{41}^s \rvert$	$\lvert p_{44}^s \rvert$
0.164	0.138	0.146	0.086	0.038	...	...	...

diffractions as a function of acoustic frequency. Here two kinds of solutions designated in the diagram respectively by "case 1" and "case 2" have been obtained for the anisotropic diffraction, for which the experiments were carried out with respect to case 1.

Inspection of Eqs. (2.36) and (2.41) reveals that in this geometry the direct photoelastic effect gives rise to anisotropic Bragg diffraction through the effective photoelastic constant

$$p_{\text{eff}}^s = |p_{41}^s \sin\theta_D - p_{66}^s \cos\theta_D| \,. \tag{2.47}$$

Recently numerical values for five of the eight independent photoelastic tensor components in tellurium were experimentally determined by the present authors,[19,20] as listed in Table I, where values for p_{14}^s, p_{41}^s, and p_{44}^s have not been determined yet. Though the actual value for p_{41}^s is still unknown, the first term on the right-hand side of Eq. (2.47) may be dropped compared to the second term, which is a good approximation as long as we are concerned with a small Bragg angle so as to satisfy the relation $\sin\theta_D \ll 1$. Then we have $p_{\text{eff}}^s \simeq |p_{66}^s|$. The absolute value of p_{66}^s can be determined from the relation[21] $|p_{66}^s| = |p_{11}^s - p_{12}^s|/2$, with $|p_{11}^s| = 0.164$ and $|p_{12}^s| = 0.138$. Because the relative sign of p_{11}^s and p_{14}^s is unknown, we shall tentatively assume the following two cases: (i) If p_{11}^s and p_{12}^s possess the same signs, then $|p_{66}^s| = 0.013$; (ii) if they possess different signs, then $|p_{66}^s| = 0.151$. The actual relative sign will be determined in Sec. III by comparing the experimentally observed diffraction intensity with those theoretically predicted from the two assumed kinds of values above.

Similarly the indirect photoelastic effect causes anisotropic Bragg diffraction through the effective photoelastic constant

$$p_{\text{eff}}^{\text{in}} = |p_{56}^{\text{in}} \sin\theta_D - p_{66}^{\text{in}} \cos\theta_D| \simeq |p_{66}^{\text{in}}| \,, \tag{2.48}$$

where Eq. (2.22) gives

$$p_{66}^{\text{in}} = -\gamma_{62} e_{26} A/\epsilon_0 \epsilon_{22} \,. \tag{2.49}$$

On the other hand, it can be easily derived that the photoelasticity arising from the free-carrier density fluctuations may give rise to isotropic Bragg diffraction via

$$p_{\text{eff}}^{\text{fc}} = |p_{16}^{\text{fc}}| = \left| -\frac{e_{26} A}{(\kappa_{11})^2 q v} \left(\frac{\kappa_{11}^n}{n_0} \frac{\omega_C^n}{1 + j(\omega/\omega_D^n)} - \frac{\kappa_{11}^p}{p_0} \frac{\omega_C^p}{1 + j(\omega/\omega_D^p)} \right) \right| . \tag{2.50}$$

In order to estimate the frequency characteristics of the two photoelastic constants predicted by Eqs. (2.48) and (2.50), the dielectric relaxation frequencies and the diffusion frequencies were determined from the Hall measurements. The sample was cut from the same crystal as used in the acousto-optic diffraction experiments in Sec. III. The Hall reversal was observed at 200°K. The estimation of μ_n and μ_p in the intrinsic region above the Hall reversal temperature was performed according to the method and formulas proposed by Grosse,[28] from which we have $n_0 \simeq p_0 = 4.4 \times 10^{15}$ cm^{-3}, $\mu_n = 1840$ cm^2/V sec, $\mu_p = 800$ cm^2/V sec, and $b = \mu_n/\mu_p = 2.3$ at room temperature. Using the low-frequency dielectric constant $\epsilon_{22} = 33$,[29] we obtain $\omega_C^n = 7.11 \times 10^{10}$ Hz, $\omega_C^p = 3.09 \times 10^{10}$ Hz, $\omega_D^n = 6.46 \times 10^7$ Hz, and $\omega_D^p = 1.49 \times 10^8$ Hz. The expected variations of $|p_{66}^{\text{in}}|$ and $|p_{16}^{\text{fc}}|$ at 10.6 μm are plotted in Fig. 3 as a function of acoustic frequency, where $\omega_M \equiv (\omega_C^n \omega_D^n)^{1/2} = (\omega_C^p \omega_D^p)^{1/2} = 2.15$

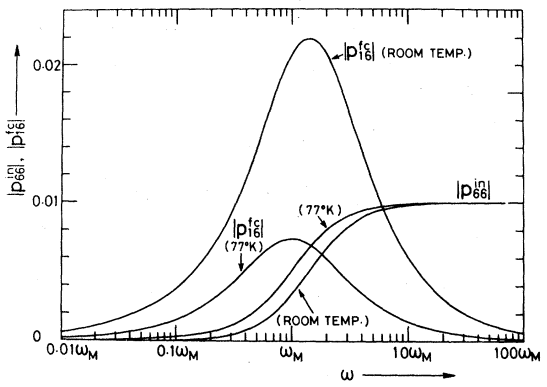

FIG. 3. Theoretical plot of $|p_{66}^{\text{in}}|$ and $|p_{16}^{\text{fc}}|$ in tellurium as a function of acoustic frequency. Calculations have been carried out for tellurium in an intrinsic region at room temperature ($\omega_M = 2.15 \times 10^9$ Hz) and in a p-type extrinsic region at 77 °K ($\omega_M = 1.0 \times 10^9$ Hz), respectively.

$\times 10^9$ Hz. The material constants used in the calculation are $e_{26} = -0.42$ C/m^2,[30] $m_n = 0.051 m_0$, $m_p = 0.146 m_0$,[31] $\kappa_{11} = N_o^2 = 22.98$,[21] and $\gamma_{62} = 6.97 \times 10^{-12}$ m/V. γ_{62} has been estimated from the nonlinear optical coefficient[32] $d_{11} = 920 \times 10^{-12}$ m/V employing Miller's rule.[33] At 77°K this sample shows p-type extrinsic conduction with $p_0 = 2.3 \times 10^{14}$ cm^{-3}, $\mu_p = 1920$ cm^2/V sec, $\omega_C^p = 3.8 \times 10^9$ Hz, $\omega_D^p = 2.7 \times 10^8$ Hz, and $\omega_M = (\omega_C^p \omega_D^p)^{1/2} = 1.0 \times 10^9$ Hz, from which $|p_{66}^{\text{in}}|$ and $|p_{16}^{\text{fc}}|$ at 77°K are calculated using Eqs. (2.30) and (2.31), as also illustrated in Fig. 3. The frequency which gives the maximum value for $|p_{16}^{\text{fc}}|$ coincides with ω_M at 77°K, while at room temperature it is shifted toward higher frequencies but still located in the range $(\omega_D^n, \omega_D^p < \omega < \omega_C^n, \omega_C^p)$. For sufficiently high frequencies $(\omega \gg \omega_D^n, \omega_D^p)$, the free-carrier bunchings attain a scale much smaller than the Debye length[10] and are effectively smeared out by thermal motion of the free carriers. The magnitude of $|p_{16}^{\text{fc}}|$ arising from the free-carrier density fluctuations is therefore considerably reduced. Figure 3 shows that the maximum attainable value for $|p_{16}^{\text{fc}}|$ is about 0.022 at the acoustic frequency of 3.03 GHz for room temperature and about 0.0074 at 1.00 GHz for 77°K. These values can be compared with the photoelastic constants listed in Table I. In the intrinsic region at room temperature, as discussed in Sec. II A, considerable cancellation may take place between p_{16}^n and p_{16}^p. To make this point clear, p_{16}^n and p_{16}^p are evaluated by resolving them into their absolute values $|p_{16}^n|$ and $|p_{16}^p|$ and the phase angle ϕ between them. The results are plotted in Fig. 4. As expected, ϕ does not deviate very much from π and shows small but maximum deviation at $\omega = 0.0457 \omega_M$. In the vicinity of the maximum of $|p_{16}^{\text{fc}}|$, about 35% of $|p_{16}^n|$ is effectively cancelled by $|p_{16}^p|$ so that the overall photoelastic constant $|p_{16}^{\text{fc}}|$ is reduced to about 65% of $|p_{16}^n|$.

On the other hand, Fig. 3 shows that $|p_{66}^{\text{in}}|$ increases monotonically with ω and, above ω_M, rapidly approaches its high-frequency limit value of 0.01.

For a given acoustic frequency the expected diffraction intensities expressed by Eq. (2.40) can be determined by knowing the Bragg angles and the relevant effective photoelastic constants. In the acousto-optic diffraction experiments carried out at room temperature in Sec. III, a shear ultrasonic wave of 120 MHz was transmitted in the y direction. At this frequency the angles of incidence and diffraction for the anisotropic Bragg diffractions are $\theta_I = 4.76°$ and $\theta_D = 6.18°$ (or, correspondingly, $\theta_I' = 23.42°$ and $\theta_D' = 31.18°$), while they are $\theta_I = \theta_D = 5.48°$ (or $\theta_I' = \theta_D' = 27.23°$) for the isotropic Bragg case. Besides, we have $p_{\text{eff}}^{\text{in}} \simeq |p_{66}^{\text{in}}| = 2.1 \times 10^{-5}$ and $p_{\text{eff}}^{\text{fc}} = |p_{16}^{\text{fc}}| = 2.5 \times 10^{-3}$ at 120 MHz. Therefore, (a) if the signs of p_{11}^s and p_{12}^s are the same,

$$I_D^d : I_D^{\text{in}} : I_D^{\text{fc}} = 1 : 2.6 \times 10^{-6} : 3.7 \times 10^{-2}; \qquad (2.51)$$

(b) if different,

$$I_D^d : I_D^{\text{in}} : I_D^{\text{fc}} = 1 : 1.9 \times 10^{-8} : 2.7 \times 10^{-4}, \qquad (2.52)$$

where I_D^d is the intensity of the diffracted light due to the direct effect, I_D^{in} is that due to the free-carrier screened indirect effect, and I_D^{fc} is that due to the free-carrier density fluctuations. The extremely small intensities of I_D^{in} may be neglected compared to I_D^d and I_D^{fc} at this acoustic frequency.

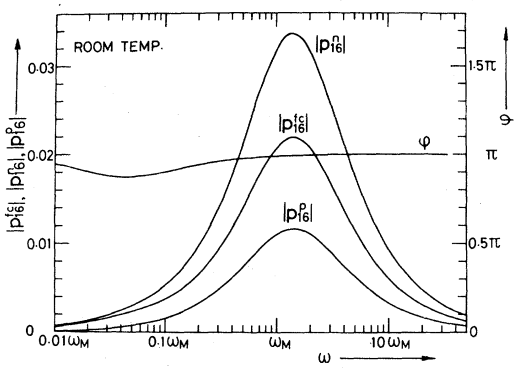

FIG. 4. Dependences of $|p_{16}^{\text{fc}}|$, $|p_{16}^n|$, $|p_{16}^p|$, and ϕ on acoustic frequency at room temperature. $|p_{16}^n|$ and $|p_{16}^p|$ are the absolute values of the photoelastic constants respectively arising from the electron- and the hole-density fluctuation, respectively. ϕ is the phase angle between p_{16}^n and p_{16}^p. $|p_{16}^{\text{fc}}|$ is equal to $|p_{16}^n + p_{16}^p|$ and therefore is obtained as their overall effect. $\omega_M = 2.15 \times 10^9$ Hz.

III. EXPERIMENTAL RESULTS AND DISCUSSION

The experiments were performed at room temperature, where tellurium shows intrinsic conduction. A schematic illustration of the experimental arrangement is given in Fig. 5. The tellurium sample was cut from a boule grown by the gradual cooling method. Since crystalline tellurium is very soft, great care was devoted to minimize a possible occurrence of damage during mechanical

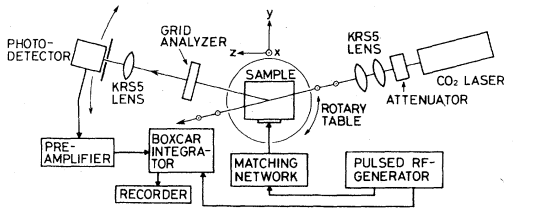

FIG. 5. Experimental arrangement for acousto-optic Bragg diffraction in tellurium. The coordinate axes denote the crystallographic orientation for the tellurium sample.

handling like cutting and abrasion. After polishing, the sample was etched by concentrated sulphuric acid at 100°C and then annealed at about 350°C for 3 days in order to remove lattice defects induced during the growth process. Finally, after the sample was subjected to the second surface polishing, slight chemical etching with concentrated sulphuric acid was again carried out to eliminate a surface damage layer. This etching process is essentially important in tellurium because optical absorption within the surface damage layer often seriously reduces its infrared transparency. The absorption coefficient of the prepared sample at 10.6 μm was about 0.5 cm^{-1} for ordinarily polarized light ($\vec{E} \perp \vec{z}$ axis) and about 4.0 cm^{-1} for extraordinarily polarized light ($\vec{E} \parallel \vec{z}$ axis), respectively. The parallelepiped sizes of the finished sample were 13.5 mm in the x direction, 7.7 mm in the y direction, and 12.5 mm in the z direction. The surface orientations were determined with respect to the cleavage plane [$(10\bar{1}0)$, hence the y plane] and believed to properly coincide with the corresponding crystallographic planes to an accuracy of much less than 1°.

For an ultrasonic transducer a selenium film epitaxially grown on the tellurium y face was used, as described by Shiosaki *et al.*,[34] by utilizing the fact that crystalline selenium possesses an isomorphic structure to tellurium. The film grown on the y face serves as a transducer which generates only shear waves propagating along the y direction. As long as the deviation of the actual sample face from the ideal crystallographic y plane is negligibly small, unexpected excitations of other unwanted acoustic modes (which often lead to serious inconvenience when using bonded shear-mode transducers, owing mainly to misoriented bonding) can be easily avoided. In the present experiments the transducer with a fundamental center frequency of about 51 MHz and fractional 3-dB bandwidth of about 90% was fabricated. The usual pulse-echo measurements carried out prior to the acousto-optic diffraction experiments proved that the time intervals of any two adjacent echoes appearing in the acoustic echo train precisely agreed with the value calculated from the shear-wave velocity, 1390 m/sec, and any noticeable spurious echo pulses ascribable to other acoustic modes were not detected. In the acousto-optic diffraction experiments the acoustic pulses with a carrier frequency of 120 MHz were excited by a pulsed rf generator utilizing the third-overtone frequency band of the transducer. The pulse width was chosen as 1 μsec.

A 10.6-μm cw CO_2 laser operating in the lowest transverse mode was used as a coherent infrared light source. The high-power output from the laser was reduced to about 20 mW with an optical attenuator in order to minimize the effects arising from light absorption. The well-collimated beam had a spot diameter of about 1 mm at the sample position. Any noticeable change was not observed in the conductivity when the sample was irradiated by light with this level of intensity. The conductivity data of the sample at room temperature have been given in Sec. II B.

A KRS5 lens focused the diffracted beam through a narrow slit mounted in front of a HgCdTe photoconductive infrared detector. The polarization direction of the laser beam was carefully adjusted by rotating the Brewster plate inserted in the laser resonator so as to align parallel to the x axis within the sample. A grid analyzer placed in front of the KRS5 lens was used to determine the polarization direction of the diffracted beam. The motor-driven rotary table on which the sample was mounted was used to obtain the angle of incidence required from the Bragg conditions as precisely as possible. The photodetector was also mechanically rotated in the y-z plane about the sample to determine the diffraction angles precisely. The signal from the photodetector was recorded after integration by the use of a Boxcar integrator.

For the present transducer, L and H in Eq. (2.40) are respectively equal to 3.5 and 11.0 mm. Under these experimental conditions we have pure Bragg diffraction because $Q \gg 4\pi$. The factor Q is equal to $(k^a)^2 L/k$ and serves as a useful criterion to determine in which regime (Bragg or Raman-Nath) the diffraction takes place[23] (where k^a and k represent respectively acoustic and optical wavenumbers in a medium). At the acoustic frequency of 120 MHz diffraction was observed for two different angles of incidence, $\theta_I' \simeq 23.9°$ and 27.1°. Figure 6 shows the angular distribution of the diffracted light intensities recorded by rotating the photodetector about about the sample for these two angles of incidence, the upper half of the figure for $\theta_I' \simeq 27.1°$ and the lower half for $\theta_I' \simeq 23.9°$. The lower half has been drawn on a vertical scale 1:100 to the upper half for the same acoustic power. The linear dependence of the diffracted light intensities on the acoustic power was carefully checked by varying the electric power applied to the transducer, so that the small-signal approximation of Eq. (2.40) was well satisfied under the present experimental conditions. In the upper half of Fig. 6 the polarization plane of the analyzer was set parallel to the polarization direction of the incident light, and the diffraction angle corresponding to the peak position was obtained as $\theta_D' \simeq 27.1° (\simeq \theta_I')$. In the lower half, on the other hand, the polarization plane of the analyzer was set

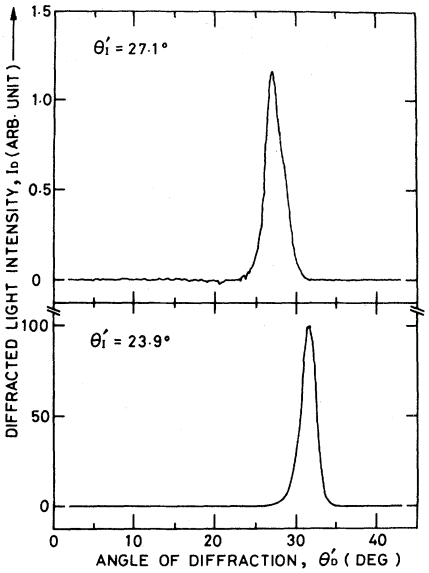

FIG. 6. Angular distribution of the diffracted light intensities measured at the same acoustic power. In the upper half of the figure the angle of incidence $\theta_I' \simeq 27.1°$ and the polarization plane of the analyzer is parallel to the polarization direction of the incident light. In the lower half $\theta_I' \simeq 23.9°$ and the polarization plane of the analyzer is normal to the polarization direction of the incident light.

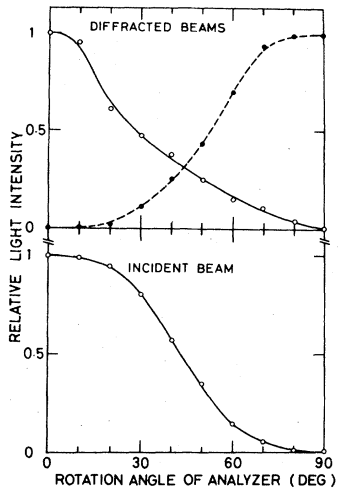

FIG. 7. Polarization states of the incident and diffracted beams determined by rotating the polarization plane of the analyzer. The solid curve in the upper half of the figure has been obtained with respect to the diffraction peak shown in the upper portion of Fig. 6, while the broken curve corresponds to the peak shown in the lower portion in Fig. 6.

normal to that of the incident light and we have $\theta_D' \simeq 31.6°$.

Figure 7 shows the polarization states of the incident and diffracted lights measured as functions of rotation angles of the analyzer. The polarization state of the incident light is plotted in the lower half of the diagram. The solid curve in the upper half was obtained with respect to the diffraction peak given in the upper half of Fig. 6, indicating that the polarization of the diffracted light is parallel to that of the incident light and hence was created by the isotropic Bragg diffraction. Quantitative agreements of the measured θ_I' and θ_D' with the calculation, i.e., $\theta_I' = \theta_D' = 27.23°$, also confirm that the diffraction arose according to the isotropic Bragg law. On the other hand, the broken curve which was obtained with respect to the diffraction peak in the lower half of Fig. 6 suggests that the polarization of the diffracted light in this case is perpendicular to that of the incident light; hence the diffraction is anisotropic, for which the calculated Bragg angles are $\theta_I' = 23.42°$, $\theta_D' = 31.18°$ and agree well with the observed angles. In addition, Fig. 6 shows that the intensity of the observed isotropic diffraction relative to the intensity of the anisotropic diffraction is about 1.2×10^{-2}.

As we have seen in Sec. II B, the isotropic diffraction observed in the experiments cannot be explained only by taking account of the direct photoelastic effect. By using the selenium transducer epitaxially grown on the moderately oriented tellurium sample, the possibility of excitation of unexpected spurious acoustic modes which might give rise to the isotropic diffraction was negligibly small. Besides, the plane of incidence and the polarization direction of the incident light had been closely adjusted. Even if we allow misalignment to a certain extent in the experimental conditions, the observed intensity of the isotropic diffraction is very much larger than that predicted solely from the direct photoelastic effect. Consequently, the possibility of an accidental contribution from the isotropic photoelastic tensor components of the direct effect, which might arise from possible experimental misorientations, can be ruled out. On the contrary, the observed relative intensity (1.2×10^{-2}) is in satisfactory agreement with the theoretically predicted one [$I_D^{tc}/I_D^d = 3.7 \times 10^{-2}$ as given in Eq. (2.51)] within a factor of 3, leading to the conclusion that the observed isotropic diffraction should be attributed to the free-carrier density fluctuations.

This is the first time that an acousto-optic diffraction due to free-carrier density fluctuations accompanying an acoustic wave has been observed in an intrinsic semiconductor. It has been shown

that this effect gives rise to an appreciable contribution to diffraction intensity in tellurium for the optical wavelength of 10.6 μm. The essential agreement of the observed diffraction intensity with the theoretical prediction given by Eq. (2.51) suggests that the signs of p_{11}^s and p_{12}^s should be the same in tellurium.

ACKNOWLEDGMENTS

The authors would like to express their thanks to Dr. J. C. Thuillier for supplying the tellurium crystal. Part of this work was supported by the Scientific Grant-in-Aids from the Ministry of Education of Japan.

[1]O. Keller, Phys. Rev. B 11, 5059 (1975).
[2]O. Keller, Phys. Rev. B 13, 4612 (1976).
[3]O. Keller, J. Opt. Soc. Am. 68, 42 (1978).
[4]D. F. Nelson and M. Lax, Phys. Rev. Lett. 24, 379 (1970).
[5]D. F. Nelson and M. Lax, Phys. Rev. B 3, 2778 (1971).
[6]V. V. Proklov, G. N. Shkerdin, and Yu. V. Gulyaev, Solid State Commun. 10, 1145 (1972).
[7]V. V. Proklov, V. I. Mirgorodsky, G. N. Shkerdin, and Yu. V. Gulyaev, Solid State Commun. 15, 1735 (1974).
[8]H. Sasaki, K. Tsubouchi, N.Chubachi, and N. Mikoshiba, J. Appl. Phys. 47, 2046 (1976).
[9]A. R. Hutson and D. L. White, J. Appl. Phys. 33, 40 (1962).
[10]J. H. McFee, *Applications to Quantum and Solid State Physics*, Vol. 4A of *Physical Acoustics: Principles and Methods*, edited by W. P. Mason (Academic, New York, 1966), p. 1.
[11]M. Fink and G. Quentin, Phys. Status Solidi A 4, 397 (1971).
[12]A. F. Gibson, Proc. Phys. Soc. London B 69, 488 (1956).
[13]T. Ishiguro and T. Tanaka, J. Phys. Soc. Jpn. 21 Suppl., 489 (1966).
[14]G. Quentin and J. M. Thuillier, Phys. Lett. 19, 631 (1966).
[15]G. Quentin and J. M. Thuillier, Solid State Commun. 4, 3 (1966).
[16]G. Quentin and J. M. Thuillier, J. Phys. Soc. Jpn. 21 Suppl., 493 (1966).
[17]T. Ishiguro and T. Tanaka, Jpn. J. Appl. Phys. 6, 864 (1967).
[18]T. Ishiguro, A. Hotta, and T. Tanaka, Jpn. J. Appl. Phys. 5, 335 (1966).
[19]S. Fukuda, T. Shiosaki, and A. Kawabata, Jpn. J. Appl. Phys. 15, 927 (1976).
[20]S. Fukuda, T. Shiosaki, and A. Kawabata, J. Appl. Phys. 50, 3899 (1979).
[21]J. F. Nye, *Physical Properties of Crystals* (Clarendon, Oxford, 1957), p. 943.
[22]N. V. Tran, Onde Electr. 47, 965 (1967).
[23]W. R. Klein and B. D. Cook, IEEE Trans. Sonics Ultrason. SU-14, 123 (1967).
[24]R. W. Dixon, IEEE J. Quantum Electron. QE-3, 85 (1967).
[25]N. Uchida and N. Niizeki, Proc. IEEE 61, 1073 (1973).
[26]D. F. Nelson and P. D. Lazay, Phys. Rev. B 6, 3109 (1972).
[27]N. Uchida and S. Saito, J. Appl. Phys. 43, 971 (1972).
[28]P. Grosse, *Springer Tracts in Modern Physics* (Springer, New York, 1969), Vol. 48, p. 144.
[29]H. Wagner, Z. Phys. 193, 218 (1966).
[30]G. Arlt and P. Quadflieg, Phys. Status Solidi 32, 687 (1969).
[31]Y. Miura and C. Hirose, J. Phys. Soc. Jpn. 33, 1522 (1972).
[32]J. H. McFee, G. D. Boyd, and P. H. Schmidt, Appl. Phys. Lett. 17, 57 (1970).
[33]R. C. Miller, Appl. Phys. Lett. 5, 17 (1964); S. H. Wemple and M. DiDominico Jr., in *Applied Solid State Science*, edited by R. Wolf (Academic, New York, 1972), Vol. III, p. 293, Eq. (7.15).
[34]T. Shiosaki, A. Kawabata, and T. Tanaka, Jpn. J. Appl. Phys. 9, 631 (1970).